Myth or reality? A disquisition concerning the photostability of bismuth-based photocatalysts

Zsolt Kása [a,*], Enikő Bárdos [b], Eszter Kása [a], Tamás Gyulavári [b], Lucian Baia [c,d], Zsolt Pap [b,c,e], Klara Hernadi [b,f]

[a] Department of Organic Chemistry, University of Szeged, Szeged, Dóm Sqr. 8. HU, 6720 Szeged, Hungary
[b] Department of Applied and Environmental Chemistry, University of Szeged, Szeged, Rerrich Béla Sqr. 1 HU, 6720 Szeged, Hungary
[c] Laboratory for Advanced Materials and Applied Technologies, Institute for Research, Development, and Innovation in Applied Natural Sciences, Fantanele 30, Cluj-Napoca RO-400294, Romania
[d] Faculty of Physics, Babeş–Bolyai University, M. Kogălniceanu Str. 1, RO-400084 Cluj–Napoca, Romania
[e] Nanostructured Materials and Bio-Nano-Interfaces Centre, Institute for Interdisciplinary Research on Bio-Nano-Sciences, Babeş–Bolyai University, RO400271, Treboniu Laurian Str. 42, Cluj-Napoca, Romania
[f] Institute of Physical Metallurgy, Metal Forming and Nanotechnology, University of Miskolc, Miskolc, H-3515, Miskolc-Egyetemváros C/1 108, Hungary

ARTICLE INFO

ABSTRACT

Photocatalysis is a well-known and extensively investigated field within advanced oxidation processes. Numerous papers have been reported that the semiconductors applied were photostable and potentially reusable based on the degradation efficiencies observed. However, researchers did not attach enough importance to investigate the residual catalysts in most cases. Here, we report on some important alterations that occurred during photocatalytic experiments, such as acid-induced and light-assisted structure break-down and complete transformation of catalysts, which could place their photostability into a new perspective. In this work, the photostability of five, increasingly popular bismuth-based oxides (Bi_2WO_6, $BiVO_4$, $BiOI$, $BiOCl$, and $BiOBr$) were investigated in the presence of various carboxylic acids (oxalic acid, formic acid, salicylic acid, malonic acid, and ascorbic acid), focusing on the crystallographic and morphological alterations of the residual photocatalysts. When investigating the resistance of the photocatalysts to oxalic acid, the formation of bismuth oxalate hydroxide was observed in all cases. At the same time, most components of the catalysts appeared in the liquid phase in high amounts. Similar transformations occurred to a lesser extent for the other acids, which was deduced to be related to the acidic strength and proton concentration. We also highlighted that in some instances, during photocatalytic processes, the occurrence of light-assisted acid-induced reactions must be considered as well.

1. Introduction

Photocatalysis is one of the most dynamically developing advanced oxidation processes. Many works focus on the modification of the commonly used, UV-active titanium dioxide [1–4] to create a visible light active material via methods such as doping [5], dye sensitization [6], or composite preparation [7]. On the other hand, visible-light-active photocatalysts have recently received greater attention all over the world, as potentially perfect alternatives for TiO_2, for instance, for the last 15–20 years, WO_3 [8], Ag_3PO_4 [9], COFs [10] or bismuth-based materials (Bi_2WO_6, $BiVO_4$, BiOX, X = Cl, Br, I) [11] have been thoroughly investigated. Bismuth-based photocatalysts became very popular

due to their beneficial properties, like excitability with visible light (narrow band gap energy), mild preparation conditions (ambient temperature, atmospheric pressure, intermediate pH, etc.), environmental compatibility, low toxicity, low cost, and last but not least, high chemical stability which was often mentioned [11–13]. However, this publication attempts to prove that bismuth-based materials are not resistant to all model pollutants, especially the carbonyl group contained materials.

Bismuth-based photocatalysts are widely used for photocatalytic water and wastewater treatment processes, gas purification, and hydrogen production resulting from water splitting [14,15]. Moreover, they show outstanding performance in degrading aqueous solutions of

---

organic pollutants, such as pharmaceuticals [16–19], dyes [20–22], or phenols [23]. Unfortunately, only a few of these publications reported the degradation of carboxyl-containing organic materials [24–28]; however, they play an important role not only in the industry but also in everyday life.

The reusability of bismuth-based materials has been investigated in the literature, and differences in photocatalytic activities have been observed several times [29–31]. Arumugam et al. studied the photocatalytic activity of modified BiOI toward tetracycline as a pollutant. After three cycles, the samples showed only 90% removal efficiency compared to the first run; however, the XRD patterns showed no change of the nanocomposites [32]. Zhu et al. investigated the photostability of modified BiOBr catalysts in Rhodamine B solution, and a minor catalytic deactivation to about 8% was experienced after the 4th run [33]. Guo et al. also reported a moderate decrease in the efficiency of the modified BiOBr, 88% of sulfamethoxazole degradation in the 5th run. The possible cause of this process can be the accumulation of the degradation intermediates on the surface of the samples, hence, blocking the active centers of the photocatalysts, stated the authors [34]. Liang et al. investigated the reusability of AgI/Bi$_2$MoO$_6$ catalyst in four consecutive cycles, and the activity slightly decreased toward E. coli cells; moreover, XRD and XPS measurements also showed vanishing differences between the samples before and after the runs [35]. Kaur and Kansal also experienced a 9% efficiency degradation of a bismuth-based catalyst, namely Bi$_2$WO$_6$ nanocuboids, against levofloxacin after three cycles [27].

In these articles the reduction of photoactivity was observed and in some studies partly discussed; however, there is no uniform explanation for this phenomenon in the literature [36,37]. Furthermore, for carboxyl group containing model pollutants, the reusability of remaining photocatalysts were not investigated at all [38,39]. There are no detailed experiments regarding the reusability and characterization of remaining photocatalyst to the authors' knowledge, where carboxyl group containing materials were used as model pollutants. The question may arise, that this is a deficiency of knowledge, or bismuth-based photocatalysts are incompatible with carboxyl-containing pollutants.

In this work, the applicability of bismuth-based photocatalysts was investigated, focusing on the degradation of carboxyl-containing compounds such as oxalic acid, ascorbic acid, salicylic acid, malonic acid, and formic acid. In addition to determining the decomposition mechanisms of different acids, the possible causes of the poor reusability were also mapped. Although this study is not focus on the photocatalytic activity itself, it can give a more comprehensive picture of the stability and reusability of bismuth-based photocatalysts (Bi$_2$WO$_6$, BiVO$_4$, BiOX, X = Cl, Br, I), hence, contributing to the determination of the real-life applicability in both industry and academics [40,41].

2. Experimental section

The used chemicals for the synthesis and photocatalytic experiments were analytical grade from Sigma-Aldrich (minimum purity: 98%) and were used without further purification. All bismuth-containing mixed oxides were synthesized by a one-step solvothermal method under similar reaction conditions. Bismuth tungstate and bismuth vanadate were crystallized in acidic media (acetic acid and nitric acid respectively) at 180 °C for 15 h according to our previous works [42,43]. For this purpose, 0.5 mM thiourea and 0.5 mM Triton X-100 were used as bismuth tungstate crystallization agents, while the pH was set to 3 with NaOH solutions in case of bismuth vanadate [43] (The molar ratios were Bi:W 2:1; Bi:V 1:1).

The BiOX-based photocatalysts were prepared as follows: bismuth nitrate pentahydrate (Bi(NO$_3$)$_3$•5 H$_2$O) was dissolved in ethylene glycol, then the necessary amounts of potassium-halides (KBr, KCl, and KI) were added to the solution (molar ratio of Bi:X = 1:1). The reaction time and temperature was 120 °C and 3 h, respectively, because using milder reaction conditions result in bismuth oxyhalides with better photocatalytic properties based on our previous work [44].

The obtained photocatalysts were characterized using X-ray diffraction (XRD; Rigaku MiniFlex Type II, Cu-Kα radiation λ = 0.15406 nm) between 20 and 80 2θ degree with a speed of 3 (2θ°) min^{-1}, and scanning electron microscopy (SEM; Hitachi 4700 Type II cold field emission electronmicroscope, accelerating voltage: 10–15 kV) to investigate morphological and crystal phase/material changes. The structure of the used materials was investigated by FT-IR spectroscopy (JASCO FT/IR-4700 spectrophotometer) equipped with a DTGS detector and ZnSe ATR accessories. The spectra were recorded in the 4000–500 cm^{-1} wavenumber range with 4 cm^{-1} resolution, and 256 scan was collected for each spectrum.

The concentration of elements in the liquid phase was measured by an Agilent 7900 inductive coupled mass spectroscope (ICP-MS), using Aristar® multielement calibration standard. High purity argon (5.5) was used as carrier gas with 15 mL·s^{-1} flow, while high purity helium (5.9) was the collision gas in the octopole reaction system (ORS). The pH of the acids was measured by a Jenway 3510 pH meter and a combined glass electrode after the electrode calibration. The photocatalytic performances of the different catalysts were tested under UV light irradiation (6 ×6 W, λ$_{max}$= 365 nm, T = 25 °C) due to test the durability. Five carboxyl-group containing organic acids, that is, oxalic acid, formic acid, malonic acid, salicylic acid, and ascorbic acid were chosen as model pollutants with 0.05 mol·L^{-1} initial concentration. The used catalyst was centrifuged and washed with Milli-Q water and absolute ethanol several times after each photocatalytic run to remove all remaining acids. The used and purified catalysts were dried at 40 °C for 24 h before the characterizations and reusability tests.

3. Results and discussion

3.1. Initial approach on the subject

BiVO$_4$ was investigated in the photocatalytic degradation of oxalic acid using the procedure described in our previous publication [43]. It was found that the sample degraded 35% of oxalic acid (Fig. 1), but a bluish solution was obtained at the end of the degradation procedure while the powder turned pale yellow. Then, the same powder was reused for another oxalic acid degradation experiment. Interestingly, the catalyst turned whiteish, while the solution turned pale blue once again, and the activity dropped to 10%. After carrying out the third reusability experiment, the powder was nearly white, while the degradation efficiency decreased to ~0%, confirming that the catalyst underwent major changes (Fig. 1).
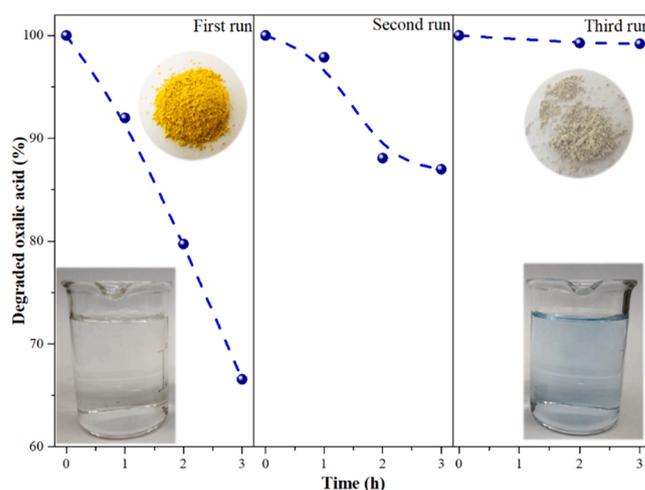
Fig. 1. Photocatalytic oxidation of oxalic acid with BiVO$_4$ and corresponding color changes. UV light irradiation was applied during the photocatalytic experiment (6 ×6 W, λ$_{max}$= 365 nm, T = 25 °C), while the initial concentration of oxalic acid was 0.05 M·L^{-1} in each run.

To elucidate the nature of the inactivation, the following blank experiments were carried out:

- The effect of oxalic acid was investigated in the dark, without irradiation, and it did not have any influence on the sample.
- The effect of light source in the absence of oxalic acid was also investigated, and the structure and morphology of the samples were unchanged.

Knowing the results of the blank experiments it was ascertained that the simultaneous presence of light source and oxalic acid was needed for the transformation to occur. Thus, the crystallographic properties of the powder were investigated after the photocatalytic experiments via XRD, and it was found that it contained several new diffraction peaks (Fig. 2/ A).

Due to the intense XRD reflections, the new material was successfully identified as bismuth oxalate hydroxide (ICDD 010–77–6175) [45], which was confirmed by HRTEM images and the calculated D-spacing parameter of the pure bismuth vanadate, and the as-prepared bismuth oxalate hydroxide (Fig. S1. in the electronic supporting information).

The photocatalytic reaction was repeated with different initial oxalic acid concentrations due to examine the effect of the pH. (Fig. 2/B). The minor reflections of the bismuth oxalate hydroxide have appeared at pH= 4.15 (5 mM oxalic acid), but decreasing absolute intensity and variable crystal facet ratio of BiVO$_4$ were observed at pH= 5.68 (0.5 mM), especially the ratio of the [040] crystal facet, which indicates that this crystal facet may be the main reaction site. Both crystal phases were detected when the initial concentration was 50 mM (pH=2.30), while the higher pH caused complete transformation after the photocatalytic experiment.

Hence, stability experiments were also carried out for the other photocatalysts to establish a pattern or a more general phenomenology.

3.2. Photocatalytic experiments using other bismuth-based photocatalysts with oxalic acid

The XRD patterns of the original photocatalysts, that is, before carrying out the photocatalytic experiments, can be seen in Fig. 3 (at the top). Bi$_2$WO$_6$ was orthorhombic (JCPDS 39–0256), BiVO$_4$ was monoclinic (JCPDS 83–1699), and the BiOX catalysts were tetragonal (BiOCl – JCPDS 82–0482; BiOBr – JCPDS 78–0348; BiOI – JCPDS 73–2062) in accordance with their respective JCPDS diffraction cards. Furthermore, the average primer crystallite size was calculated by the Scherrer equation (Table S1 in Electronic supporting information).

The micromorphological properties were also investigated before and after the photocatalytic reactions via SEM. The morphology was

diverse: for most samples, 3D flower-like microsphere shapes were observed with an average particle diameter of 2–4 µm. The only exception was BiVO$_4$, which consisted of plates with 1.5 µm average particle size (detailed in our previous publications [42–44]).

After testing with oxalic acid, most of these structures changed drastically; seemingly, only the morphology of Bi$_2$WO$_6$ remained intact. The hierarchical microsphere shape of the bismuth oxyhalides became a rod-like structure, which arranged into a star-like shape. The bismuth vanadate transformed from a plate-like structure to rod-like particles similar to the previous one, while the original flower-like morphology of bismuth tungstate did not change, but a few rod-like particles appeared.

The new diffraction peaks, which were detected at the exact locations in all cases at 20.7 and 22.1 2θ degree, suggest that all samples underwent structural transformations after the photocatalytic experiments. Furthermore, the transformations of bismuth oxyhalides were nearly complete, because of the original diffraction peaks were not clearly detectable. The formed new materials were identified as the same orthorhombic bismuth oxalate hydroxide (Bi(C$_2$O$_4$)OH: ICDD 010–77–6175) as it was previously mentioned for bismuth vanadate. It is important to highlight that bismuth oxalate hydroxide also could possess photocatalytic activity, as Xiao and co-workers have already published [46].

3.3. Infrared spectroscopy studies

The transformation was monitored by infrared spectroscopy. The bismuth vanadate was suspended in oxalic acid solution with different concentrations (0.05–100 mM), and 3 h of UV light irradiation was applied. For BiVO$_4$ (Fig. 4/A), a characteristic peak of the V–O bond was detected at 610 cm^{-1}, but with increasing oxalic acid quantity, this peak intensity decreased, while a Bi–O band intensity at 512 cm^{-1} got to be more pronounced [47]. Simultaneously, the envelope curve of the symmetric and asymmetric carboxylate vibrations arises between 1380 cm^{-1} to 1694 cm^{-1} after adding more than 5 mM oxalic acid to the suspensions. The differences ($\Delta\nu= 121$ cm^{-1}) between $\nu_{sym.}$ and $\nu_{as.}$ suggests, that the carboxylate group is present as a bidentate ligand. Moreover, the signal at 791 cm^{-1} corresponds to the planar bending vibrations of carboxylate groups $\delta_{(COO-)}$, while at 1294 cm^{-1} and 1355 cm^{-1}, the stretching vibrations $\nu_{(C-O)}$ of bismuth oxalate are visible. The stretching vibrations of the C=O at 1712 cm^{-1} indicate of hydrogen bonds between the oxalate groups. It is also confirmed by shifting the stretching vibration bands $\nu_{(HO-)}$ at 1086 cm^{-1} [45].

The infrared spectra of the other photocatalysts (Bi$_2$WO$_6$, BiOX) were also recorded after the photocatalytic reaction with 50 mM oxalic acid (Fig. 4/B). The IR spectra were very similar to the photocatalytically used bismuth vanadate (signal position, $\Delta\nu$ etc.). However, a weak
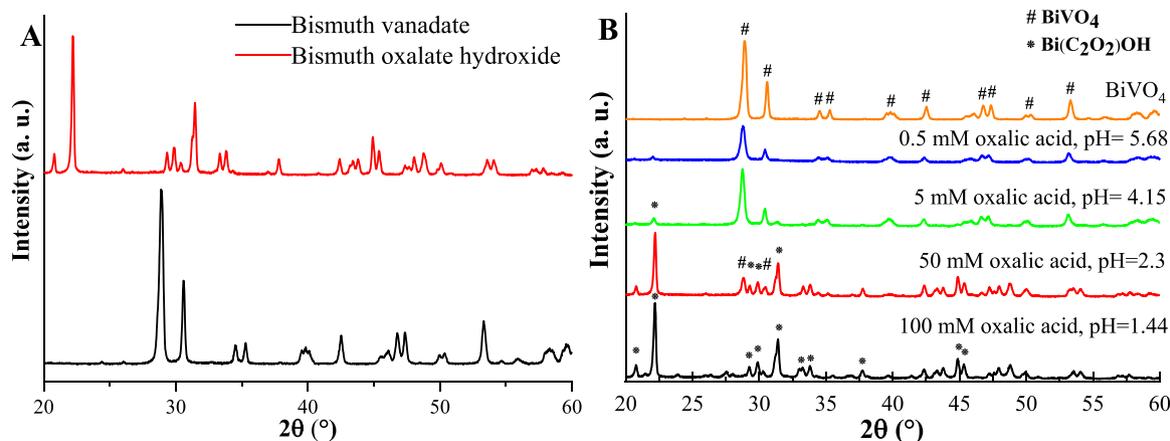
Fig. 2. XRD patterns of bismuth vanadate before the photocatalytic experiments and its transformation after the third run (A). The completely transformed material was identified as bismuth oxalate hydroxide (ICDD 010–77–6175). The effect of the pH on the XRD pattern of the end-product (**B**).
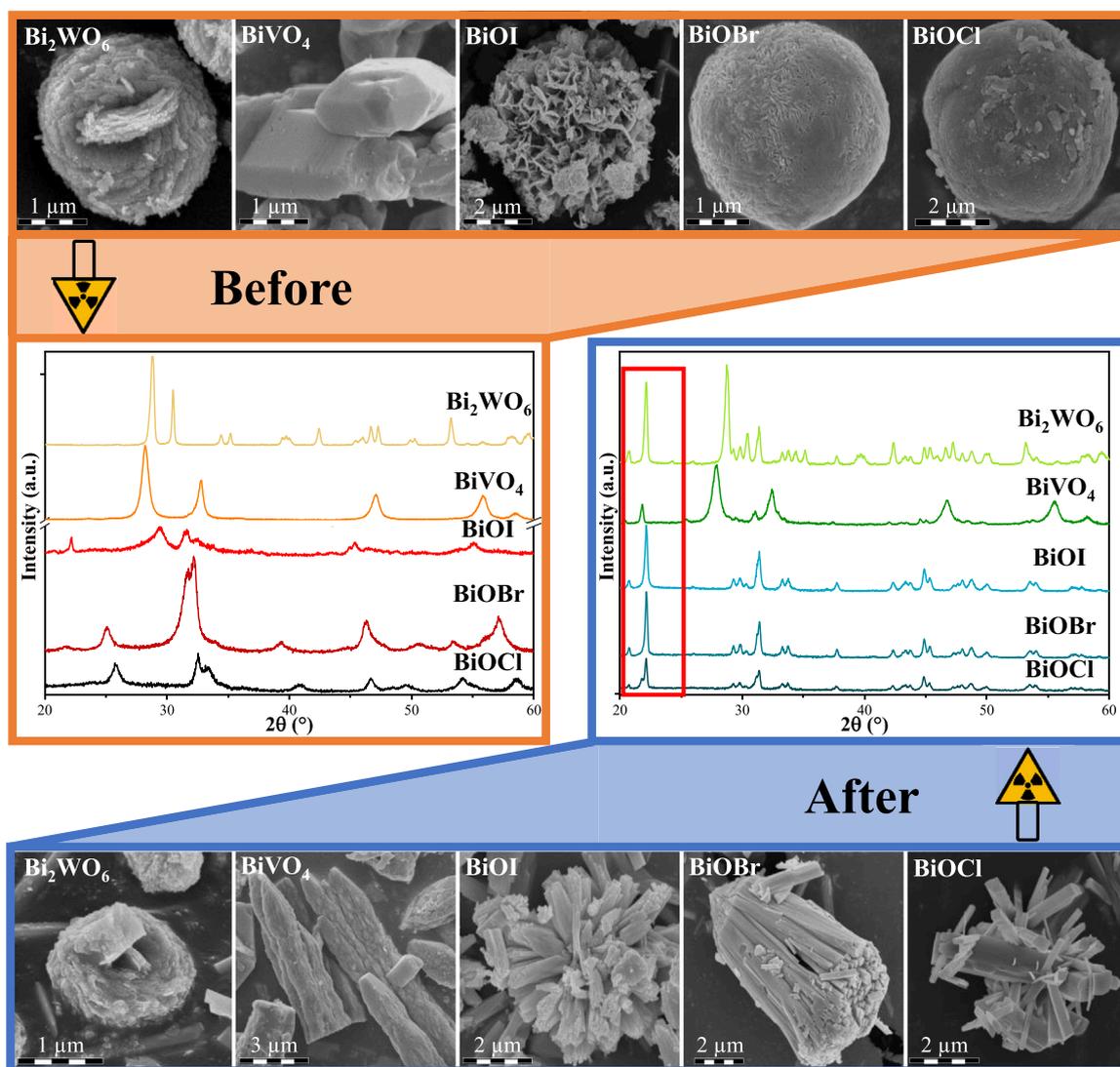
Fig. 3. Scanning electron microscope images and X-ray diffraction patterns of the catalysts before and after 3 h of photoreactions with oxalic acid.

additional adsorption band was detected at 699 cm^{-1} is assigned to the asymmetrical stretching vibrations of Bi–O bonds and may originated to the BiOX [48]. This is a clear confirmation that the same kind of bismuth oxalate hydroxide was formed after the photocatalytic reactions.

3.4. Photocatalytic reactions of bismuth-based photocatalysts with different carboxylic acids

After the interesting outcome of the tests using oxalic acid, the stabilities of bismuth-based photocatalysts were further investigated. For this purpose, two simple (the malonic acid, which is an oxalic acid analogue, the formic acid as a hard-to-deal acid) and two more complex (ascorbic acid as radical scavenger and salicylic acid as a well-known model pollutant and complexing agent) carboxylic acids were used. The goal of these experiments was to reveal whether the transformation mentioned before is an individual case, or whether it also occurs with other acids.

As it can be seen in Fig. 5, the simple acids did not significantly influence the morphology of the particles. Only one exception was observed: malonic acid changed the morphology of Bi_2WO_6 from 3D hierarchical spheres to the distorted cluster of nanoplates. For BiOI, the original structure remained intact in most cases, but formic acid and salicylic acid caused significant morphological changes: some sharp thorn-like crystals appeared after the photocatalytic reaction. The

morphology of the other BiOX photocatalysts did not change, but the surface became very smooth; no individual crystals were detectable. Furthermore, malonic acid and ascorbic acid caused the aggregation of particles. Based on the photographs (Fig. 5 *insets*), a significant transformation occurred during the photocatalytic experiments, namely, the color of the catalysts was changed. BiOCl and BiOBr turned to greyish or blackish, while BiOI faded in color significantly.

These observations may suggest that only surface-related changes occurred while the crystal structure remained intact. Based on Fig. S2, the XRD patterns of the end-products did not show significant differences compared to that of the original ones. New reflections did not appear as in the case of oxalic acid, only a slight decrease in intensity was observed, and some diffraction peaks merged. Interestingly, the XRD patterns of bismuth tungstate and vanadate remained unchanged. This may suggest that the structures of BiOX are less stable against organic acids (and against light) than those of Bi_2WO_6 and $BiVO_4$. The calculated primer crystallite sizes (Table S1) were not changed significantly or decreased slightly after the photocatalytic reaction, which confirmed that the investigated carboxylic acid in this concentration could not disintegrate the crystal structure.

3.5. Elemental analysis of residual solutions

Due to the blue color of the supernatant observed for $BiVO_4$, the
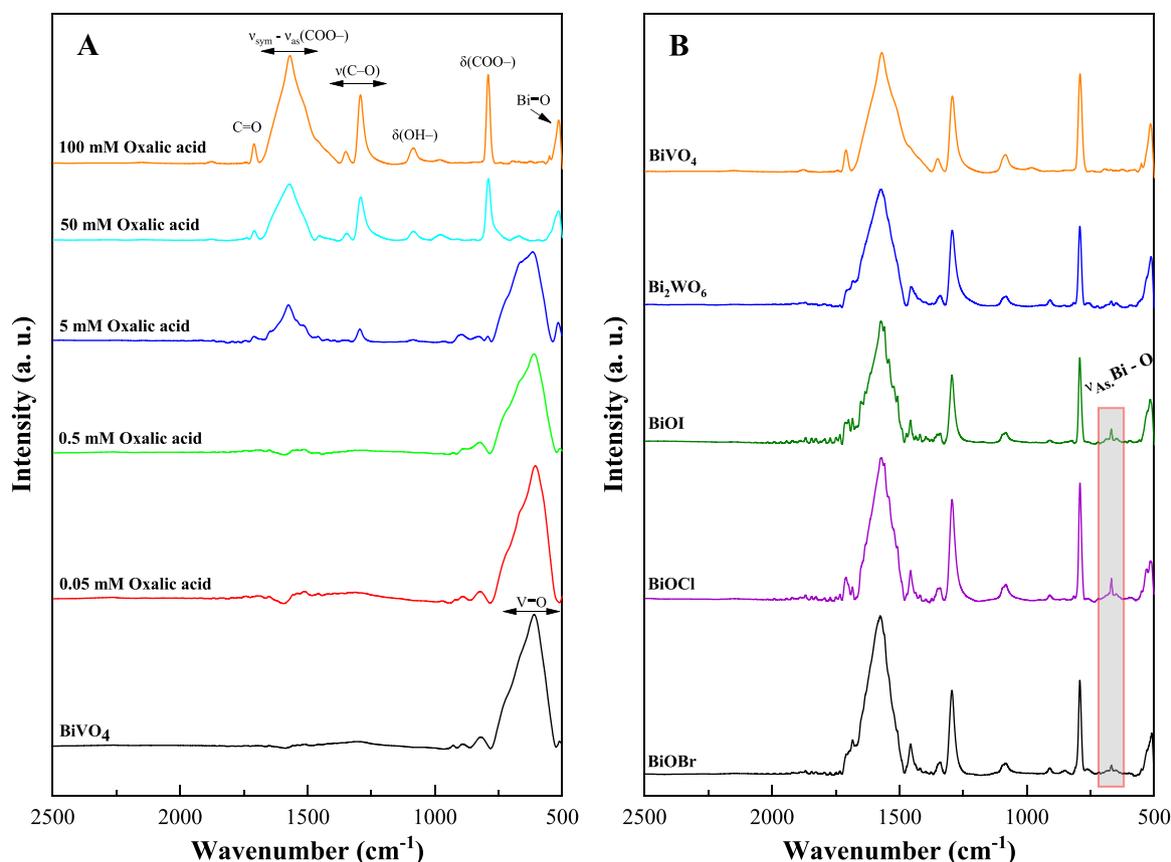
Fig. 4. Infrared spectra from the bismuth-based materials after the photocatalytic reactions with oxalic acid. A: $BiVO_4$ + different concentrations of oxalic acid, **B:** bismuth-based photocatalysts + 50 mM oxalic acid.

liquid phase of each sample was investigated. After the photocatalytic reactions, the liquids were centrifuged, filtered (0.45 μm), diluted, and all possible atoms (Bi, V, W, Cl, Br, I) were monitored directly by ICP-MS to find out which acid could break down the structure of the catalysts.

First, bismuth vanadate and its photocatalytic reaction with oxalic acid was examined (Fig. 6), while monitoring the V and Bi elements. The measured element concentrations were converted to weight percentages to determine the proportion of the dissolved elements. During the first run, the concentration of vanadium ions was increasing, which continued to increase during the second and third runs. By the end of the third run, all of the vanadium ions entered the liquid phase. Interestingly, the bismuth content also increased slightly, but only for the first measured points each run. This may indicate an equilibrium process, where the bismuth ions were reduced to the surface of the catalysts, thereby enabling electron transfer to the vanadyl ions. This suggests that the transformation of bismuth oxalate hydroxide was a multi-step process, where the decay of structure was the first step.

The resistance of the other photocatalysts to oxalic acid was also investigated. The ICP-MS results in Table 1 and Table 2 corroborated our previous assumption that BiOX photocatalysts were less stable against oxalic acid. This is because more than 90% of the halides (I: 93.2%, Cl: 98.7%, Br: 99.9%) entered the liquid phase, while the concentration of tungsten was lower (10.8%). Interestingly, the bismuth content was relatively high for bismuth tungstate (9.8%).

The resistance of the photocatalysts against the other model pollutants (i.e., formic acid, malonic acid, salicylic acid, and ascorbic acid) was also investigated. The concentrations of elements were measured after 3 h of UV light irradiation (Tables 1 and 2). It was ascertained that they did not change significantly; even so, iodine appeared in large quantities in the presence of each model pollutant. These results could also mean that the resistance of bismuth-based catalysts is greater to the

other carboxylic acids than to oxalic acid, which may be related to the proton concentration. Consequently, the pH values of the acids were also measured before and after the photocatalytic experiments (Table S2). Increasing pH values were observed only for $BiVO_4$ and Bi_2WO_6 in oxalic acid after 3 h (2.35–2.71 and 2.68 respectively), which means that these reactions consumed protons.

3.6. Possible transformation mechanism

Based on the results obtained, a plausible explanation was provided regarding the possible transformations and potential mechanisms. Summarizing the results for $BiVO_4$, the pH increased, and vanadium ions appeared in the liquid phase after 3 h of photocatalytic oxidation. Consequently, the authors propose the following simplified reactions:

$$BiVO_4 + HC_2O_4^- \rightarrow Bi(C_2O_4)OH + VO_3^- \tag{1}$$

$$VO_3^- + 4\,H^+ + (\text{photogenerated})\,e^- \rightarrow VO^{2+} + 2\,H_2O \tag{2}$$
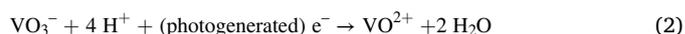
where the oxalic acid was in single deprotonated form in this pH range [49], the photogenerated electron originating from the excitation of $BiVO_4$ and the $Bi(C_2O_4)OH$ formed during this process jointly caused the reduction of vanadate and formation of water at the same time. This process went on until one of the limiting components ran out. If we consider the pH values before and after the reaction, the proton concentration defines the reaction rate and the endpoint of the reduction. When the proton content was restored with additional oxalic acid (second and third run) the rate of vanadate reduction increased again. Consequently, the formation of bismuth oxalate hydroxide from bismuth vanadate is a light-assisted, acid-induced reaction, where the proton concentration is the limiting factor. The key to the reaction may be the adsorption of singly deprotonated oxalic acid on the surface. The
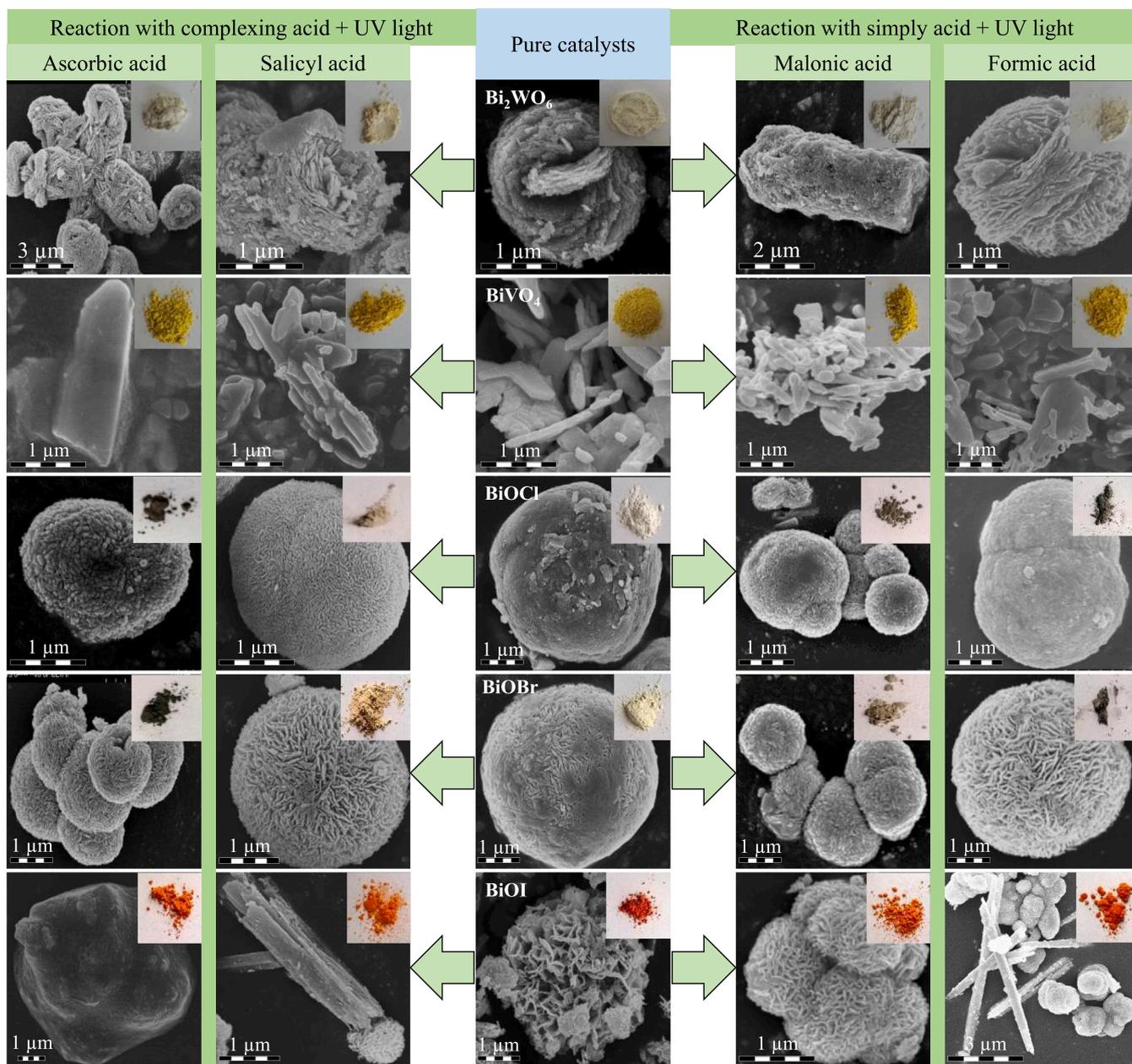
Fig. 5. SEM micrographs and photographs (**insets**) of the bismuth-based photocatalysts before and after photocatalytic treatment in the presence of different organic acids.

proposed light-assisted acid-induced transformation mechanism is as follows:

(1) Adsorption of singly deprotonated oxalic acid, and surface complexation of oxalate with Bi^{3+};
(2) Light excitation, electron–hole separation;
(3) Reduction of vanadate ions and disintegration of structure;
(4) Formation of bismuth oxalate hydroxide.

For bismuth oxyhalides, the following photoreduction reaction (Eq. 3) is already known in the literature [50]:

$$BiOX + 2\,H^+ + 3e^- \rightarrow Bi^0 + X^- + H_2O \quad (3)$$

$$BiOX + 2\,H^+ + 3e^- + H(C_2O_2)^- \rightarrow Bi(C_2O_2)OH + X^- + 2\,H^+ + 3e^- \quad (4)$$

$$e^- + O_2 \rightarrow O_2^{\bullet-} \quad (5)$$
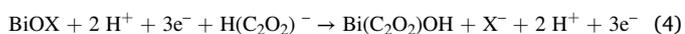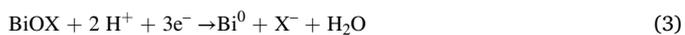
In our system, the deprotonation of oxalic acid could ensure the proton concentration, while the photogenerated electron could contribute to the disintegrate of the structure. After the BiOX layers came apart alongside of the van der Waals bonds, the Bi-oxalate complex could form on the surface (Eq. 4), and prevent the reduction of bismuth. Thereby, the photogenerated electron could facilitate radical formation and degrade the remaining oxalic acid because the dissolved oxygen could be an effective electron acceptor (Eq. 5) [51]. This may explain that the pH of the oxalic acid solution was not changed after the photocatalytic run. However, due to the disintegrated structure and Bi-oxalate complex and hydroxide, the halides remained in the solution. Consequently, this transformation could be considered a light-assisted, acid-induced ion exchange process.

The reaction of oxalic acid with bismuth tungsten may be very similar to that with BiOX, but presumably WO_4^{2-} receives a proton and forms HWO_4^- (Eq. 6) or may form a single protonated polytungstate anion, such as $HW_{12}O_{39}^{5-}$, $HW_{12}O_{41}^{9-}$, or $HW_6O_{20}(OH)^{4-}$ [52,53].
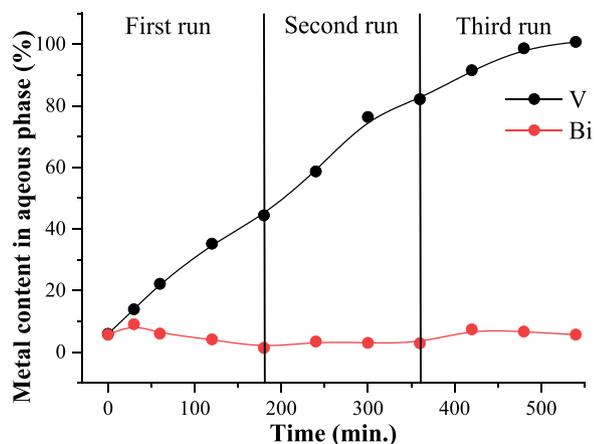
Fig. 6. Photocatalytic degradation curves of oxalic acid using bismuth vanadate under UV light irradiation. The total vanadium and bismuth contents were monitored by ICP-MS in the aqueous phase. The initial concentration of oxalic acid was 0.05 M·L^{-1} in each run.

Table 1
The element content of the aqueous phase compared to the element content of the solid phase after 3 h of photocatalytic reaction with oxalic acid.

Organic acid	BiVO$_4$	Bi$_2$WO$_6$	BiOI	BiOCl	BiOBr
	$V_{aq}/V_{tot.}$ (%)	$W_{aq}/W_{tot.}$ (%)	$I_{aq}/I_{tot.}$ (%)	$Cl_{aq}/Cl_{tot.}$ (%)	$Br_{aq}/Br_{tot.}$ (%)
Oxalic acid	44.4	10.8	93.2	98.7	99.9
Salicylic acid	0.8	0.1	44.9	1.1	2.8
Ascorbic acid	2.6	1.2	17.7	3.2	4.5
Formic acid	0.6	0.5	9.2	1.0	2.5
Malonic acid	0.9	0.5	5.6	0.9	1.2

Table 2
Bismuth content of the aqueous phase compared to the element content of the solid phase after 3 h photocatalytic reaction of different organic acid.

Organic acid	BiVO$_4$	Bi$_2$WO$_6$	BiOI	BiOCl	BiOBr
	$Bi_{aq}/Bi_{tot.}$ (%)				
Oxalic acid	1.3	9.8	0.5	0.5	0.3
Salicylic acid	0.1	0.4	1.4	0.2	0.2
Ascorbic acid	2.2	2.7	2.0	1.3	0.8
Formic acid	0.1	1.3	0.4	0.2	0.3
Malonic acid	0.2	1.1	0.3	0.1	0.1

Furthermore, tungsten can coordinate to two oxalate ions; consequently, the process of metal-oxalate complexation may compete with that of precipitation, which explains the higher bismuth content in the liquid phase (Table 2).

$$Bi_2WO_6 + 2HC_2O_4^- \rightarrow 2Bi(C_2O_4)OH + WO_4^{2-} \tag{6}$$

The other acids had higher pH values, thus lower proton concentrations, which did not change after 3 h of light irradiation (Table S2). Consequently, the analogues of the acid-induced reactions described above occurred only to a lesser extent, because of the lack of critical proton concentration. Nonetheless, surface reactions may occur during photocatalytic reactions.

4. Conclusions

In this work, the photostability of different bismuth-based photocatalysts was investigated in the presence of different carboxylic acids. It

was ascertained that the acids reacted with the semiconductors and broke down their structure to different extents. Consequently, the constituents making up the catalysts (such as vanadate, tungstate, iodine, chlorine, bromine, and bismuth) entered the liquid phase, which was proven by ICP-MS measurements. According to the ICP-MS and XRD results, this transformation is especially typical for oxalic acid, while the other acid caused only moderate transformations. It was proposed that this transformation could be caused by the photogenerated electron, the proton concentration, and the potential of bismuth to form stable complexes with carbonyl group containing acids. In the light of our results, the authors suggest that more comprehensive investigations are required in all cases where the goal is to examine reusability. Moreover, close attention should be paid to the investigation of liquid phases for any bismuth-based photocatalysts. Investigating other carbonyl group containing model pollutants in terms of pH can also raise exciting question about whether bismuth-based semiconductors can really be used as photocatalysts.

CRediT authorship contribution statement

Zsolt Kása: Conceptualization, Methodology, Data curation, Original draft preparation, **Enikő Bárdos:** Investigation, Data curation, Writing, **Eszter Kása:** Investigation, Data curation, Visualization, Writing, **Tamás Gyulavári:** Investigation, Data visualization, Reviewing, **Lucian Baia:** Supervision, Reviewing, **Zsolt Pap:** Supervision, Reviewing, Conceptualization, **Klara Hernadi:** Supervision, Reviewing, Funding.

Declaration of Competing Interest

The authors declare that they have no known competing financial interests or personal relationships that could have appeared to influence the work reported in this paper.

Appendix A. Supporting information

Supplementary data associated with this article can be found in the online version at doi:10.1016/j.jece.2022.107624.

References

[1] J.J. Rueda-Marquez, I. Levchuk, P. Fernández Ibañez, M. Sillanpää, A critical review on application of photocatalysis for toxicity reduction of real wastewaters, J. Clean. Prod. 258 (2020) 120694, https://doi.org/10.1016/j.jclepro.2020.120694.

[2] A. Fujishima, T.N. Rao, D.A. Tryk, Titanium dioxide photocatalysis, J. Photochem. Photobiol. C Photochem. Rev. 1 (2000) 1–21, https://doi.org/10.1016/S1389-5567(00)00002-2.

[3] Q. Guo, C. Zhou, Z. Ma, X. Yang, Fundamentals of TiO$_2$ photocatalysis: concepts, mechanisms, and challenges, Adv. Mater. 31 (2019) 1901997, https://doi.org/10.1002/adma.201901997.

[4] D. Ma, J. Li, A. Liu, C. Chen, Carbon gels-modified TiO$_2$: promising materials for photocatalysis applications, Materials 13 (2020) https://doi.org/:173410.3390/ma13071734.

[5] H. Sudrajat, S. Babel, A.T. Ta, T.K. Nguyen, Mn-doped TiO$_2$ photocatalysts: role, chemical identity, and local structure of dopant, J. Phys. Chem. Solids 144 (2020) 109517, https://doi.org/10.1016/j.jpcs.2020.109517.

[6] M. Ghosh, P. Chowdhury, A.K. Ray, Photocatalytic activity of aeroxide TiO2 sensitized by natural dye extracted from mangosteen peel, Catalysts 10 (2020) 917, https://doi.org/10.3390/catal10080917.

[7] Y. Song, J. Zhang, L. Yang, S. Cao, H. Yang, J. Zhang, L. Jiang, Y. Dan, P. Le Rendu, T.P. Nguyen, Photocatalytic activity of TiO₂ based composite films by porous conjugated polymer coating of nanoparticles, Mater. Sci. Semicond. Process. 42 (2016) 54–57, https://doi.org/10.1016/j.mssp.2015.06.078.

[8] I.M. Szilágyi, B. Fórizs, O. Rosseler, Á. Szegedi, P. Németh, P. Király, G. Tárkányi, B. Vajna, K. Varga-Josepovits, K. László, A.L. Tóth, P. Baranyai, M. Leskelä, WO₃ photocatalysts: influence of structure and composition, J. Catal. 294 (2012) 119–127, https://doi.org/10.1016/j.jcat.2012.07.013.

[9] C.-S. Tseng, T. Wu, Y.-W. Lin, Facile synthesis and characterization of Ag3PO4 microparticles for degradation of organic dyestuffs under white-light light-emitting-diode irradiation, Materials (2018) 708.

[10] Y. Qian, D. Ma, Covalent organic frameworks: new materials platform for photocatalytic degradation of aqueous pollutants, Materials 14 (2021) 5600, https://doi.org:10.3390/ma14195600.

[11] L. Zhang, Y. Li, Q. Li, J. Fan, S.A.C. Carabineiro, K. Lv, Recent advances on Bismuth-based photocatalysts: strategies and mechanisms, Chem. Eng. J. 419 (2021) 129484, https://doi.org/10.1016/j.cej.2021.129484.

[12] L. Ye, Y. Deng, L. Wang, H. Xie, F. Su, Bismuth-based photocatalysts for solar photocatalytic carbon dioxide conversion, ChemSusChem 12 (2019) 3671–3701, https://doi.org:10.1002/cssc.201901196.

[13] R. Kumar, P. Raizada, N. Verma, A. Hosseini-Bandegharaei, V.K. Thakur, Q.V. Le, V.-H. Nguyen, R. Selvasembian, P. Singh, Recent advances on water disinfection using bismuth based modified photocatalysts: strategies and challenges, J. Clean. Prod. 297 (2021), 126617, https://doi.org/10.1016/j.jclepro.2021.126617.

[14] C. Martinez Suarez, S. Hernández, N. Russo, BiVO4 as photocatalyst for solar fuels production through water splitting: a short review, Appl. Catal. A: Gen. 504 (2015) 158–170, https://doi.org/10.1016/j.apcata.2014.11.044.

[15] G.-J. Lee, Y.-C. Zheng, J.J. Wu, Fabrication of hierarchical bismuth oxyhalides (BiOX, X = Cl, Br, I) materials and application of photocatalytic hydrogen production from water splitting, Catal. Today (2017) https://doi.org:10.1016/j.cattod.2017.04.044.

[16] J.C. Ahern, R. Fairchild, J.S. Thomas, J. Carr, H.H. Patterson, Characterization of BiOX compounds as photocatalysts for the degradation of pharmaceuticals in water, Appl. Catal. B Environ. 179 (2015) 229–238, https://doi.org:10.1016/j.apcatb.2015.04.025.

[17] R.P. Panmand, Y.A. Sethi, S.R. Kadam, M.S. Tamboli, L.K. Nikam, J.D. Ambekar, C.-J. Park, B.B. Kale, Self-assembled hierarchical nanostructures of Bi₂WO₆ for hydrogen production and dye degradation under solar light, CrystEngComm 17 (2015) 107–115, https://doi.org/10.1039/C4CE01968G.

[18] W. Shi, Y. Yan, X. Yan, Microwave-assisted synthesis of nano-scale BiVO4 photocatalysts and their excellent visible-light-driven photocatalytic activity for the degradation of ciprofloxacin, Chem. Eng. J. (215–216) (2013) 740–746, https://doi.org/10.1016/j.cej.2012.10.071.

[19] Y. Zhiyong, D. Bahnemann, R. Dillert, S. Lin, L. Liqin, Photocatalytic degradation of azo dyes by BiOX (X⎯Cl, Br), J. Mol. Catal. A: Chem. 365 (2012) 1–7, https://doi.org/10.1016/j.molcata.2012.07.001.

[20] L. Ge, Novel visible-light-driven Pt/BiVO4 photocatalyst for efficient degradation of methyl orange, J. Mol. Catal. A: Chem. 282 (2008) 62–66, https://doi.org/10.1016/j.molcata.2007.11.017.

[21] X. Qin, H. Cheng, W. Wang, B. Huang, X. Zhang, Y. Dai, Three dimensional BiOX (X⎯Cl, Br and I) hierarchical architectures: facile ionic liquid-assisted solvothermal synthesis and photocatalysis towards organic dye degradation, Mater. Lett. 100 (2013) 285–288, https://doi.org/10.1016/j.matlet.2013.03.045.

[22] Z. Zhang, W. Wang, M. Shang, W. Yin, Low-temperature combustion synthesis of Bi₂WO₆ nanoparticles as a visible-light-driven photocatalyst, J. Hazard Mater. 177 (2010) 1013–1018, https://doi.org/10.1016/j.jhazmat.2010.01.020.

[23] Z. Li, X. Meng, New insight into reactive oxidation species (ROS) for bismuth-based photocatalysis in phenol removal, J. Hazard. Mater. 399 (2020), 122939, https://doi.org/10.1016/j.jhazmat.2020.122939.

[24] B. Sarwan, B. Pare, A.D. Acharya, Heterogeneous photocatalytic degradation of nile blue dye in aqueous BiOCl suspensions, Appl. Surf. Sci. 301 (2014) 99–106, https://doi.org/10.1016/j.apsusc.2014.01.136.

[25] L. Dong, S. Guo, S. Zhu, D. Xu, L. Zhang, M. Huo, X. Yang, Sunlight responsive BiVO4 photocatalyst: Effects of pH on L-cysteine-assisted hydrothermal treatment and enhanced degradation of ofloxacin, Catal. Commun. 16 (2011) 250–254, https://doi.org/10.1016/j.catcom.2011.05.005.

[26] X. Xiong, L. Ding, Q. Wang, Y. Li, Q. Jiang, J. Hu, Synthesis and photocatalytic activity of BiOBr nanosheets with tunable exposed {010} facets, Appl. Catal. B Environ. 188 (2016) 283–291, https://doi.org/10.1016/j.apcatb.2016.02.018.

[27] A. Kaur, S.K. Kansal, Bi₂WO₆ nanocuboids: an efficient visible light active photocatalyst for the degradation of levofloxacin drug in aqueous phase, Chem. Eng. J. 302 (2016) 194–203, https://doi.org/10.1016/j.cej.2016.05.010.

[28] M. Long, P. Hu, H. Wu, Y. Cai, B. Tan, B. Zhou, Efficient visible light photocatalytic heterostructure of nonstoichiometric bismuth oxyiodide and iodine intercalated Bi₂O₂CO₃, Appl. Catal. B Environ. 184 (2016) 20–27, https://doi.org:10.1016/j.apcatb.2015.11.025.

[29] H. Shi, Y. Zhao, J. Fan, Z. Tang, Construction of novel Z-scheme flower-like Bi₂S₃/SnIn₄S₈ heterojunctions with enhanced visible light photodegradation and bactericidal activity, Appl. Surf. Sci. 465 (2019) 212–222, https://doi.org/10.1016/j.apsusc.2018.09.164.

[30] H. Zhai, J. Kong, A. Wang, H. Li, T. Zhang, A. Li, D. Wu, The polymerization effect on synthesis and visible-light photocatalytic properties of low-temperature β-BiNbO4 using Nb-citrate precursor, Nanoscale Res. Lett. 10 (2015) 457, https://doi.org/10.1186/s11671-015-1165-z.

[31] Y. Yao, J. Liang, Y. Wei, X. Zheng, X. Xu, G. He, H. Chen, One-pot synthesis of visible-light-driven photocatalyst for degradation of Rhodamine B: graphene based

[32] M. Arumugam, S.J. Lee, T. Begildayeva, S.S. Naik, Y. Yu, H. Lee, J. Theerthagiri, M. Y. Choi, Enhanced photocatalytic activity at multidimensional interface of 1D-Bi₂S₃@2D-GO/3D-BiOI ternary nanocomposites for tetracycline degradation under visible-light, J. Hazard. Mater. 404 (2021), 123868, https://doi.org/10.1016/j.jhazmat.2020.123868.

[33] S.-R. Zhu, Q. Qi, W.-N. Zhao, M.-K. Wu, Y. Fang, K. Tao, F.-Y. Yi, L. Han, Hierarchical core–shell SiO₂@PDA@BiOBr microspheres with enhanced visible-light-driven photocatalytic performance, Dalton Trans. 46 (2017) 11451–11458, https://doi.org:10.1039/C7DT01581J.

[34] F. Guo, J. Chen, J. Zhao, Z. Chen, D. Xia, Z. Zhan, Q. Wang, Z-scheme heterojunction g-C₃N₄@PDA/BiOBr with biomimetic polydopamine as electron transfer mediators for enhanced visible-light driven degradation of sulfamethoxazole, Chem. Eng. J. 386 (2020), 124014, https://doi.org/10.1016/j.cej.2020.124014.

[35] J. Liang, F. Liu, J. Deng, M. Li, M. Tong, Efficient bacterial inactivation with Z-scheme AgI/Bi₂MoO₆ under visible light irradiation, Water Res. 123 (2017) 632–641, https://doi.org/10.1016/j.watres.2017.06.060.

[36] E. da Cruz Severo, G.L. Dotto, A. Martínez-de la Cruz, E.L. Cuellar, E.L. Foletto, Enhanced photocatalytic activity of BiVO4 powders synthesized in presence of EDTA for the decolorization of rhodamine B from aqueous solution, Environ. Sci. Pollut. Res. 25 (2018) 34123–34130, https://doi.org:10.1007/s11356-018-3370-7.

[37] H. Fu, C. Pan, W. Yao, Y. Zhu, Visible-light-induced degradation of rhodamine B by nanosized Bi₂WO₆, J. Phys. Chem. B 109 (2005) 22432–22439, https://doi.org/:10.1021/jp052995j.

[38] K. Pingmuang, N. Wetchakun, W. Kangwansupamonkon, K. Ounnunkad, B. Inceesungvorn, S. Phanichphant, Photocatalytic mineralization of organic acids over visible-light-driven Au/BiVO4 photocatalyst, Int. J. Photo 2013 (2013), 943256 https://doi.org:/10.1155/2013/943256.

[39] X. Liu, Z. Guo, L. Zhou, J. Yang, H. Cao, M. Xiong, Y. Xie, G. Jia, Hierarchical biomimetic BiVO4 for the treatment of pharmaceutical wastewater in visible-light photocatalytic ozonation, Chemosphere 222 (2019) 38–45, https://doi.org/10.1016/j.chemosphere.2019.01.084.

[40] L. Candish, K.D. Collins, G.C. Cook, J.J. Douglas, A. Gómez-Suárez, A. Jolit, S. Keess, Photocatalysis in the life science industry, Chem. Rev. 122 (2022) 2907–2980, https://doi.org:/10.1021/acs.chemrev.1c00416.

[41] Z. Kása, E. Orbán, Z. Pap, I. Ábrahám, K. Magyari, S. Garg, K. Hernadi, Innovative and cost-efficient BiOI immobilization technique on ceramic paper—total coverage and high photocatalytic activity, Nanomaterials 10 (2020) 1959, https://doi.org/:10.3390/nano10101959.

[42] Z. Kása, K. Saszet, A. Dombi, K. Hernádi, L. Baia, K. Magyari, Z. Pap, Thiourea and Triton X-100 as shape manipulating tools or more for Bi₂WO₆ photocatalysts? Mater. Sci. Semicond. Process. 74 (2018) 21–30, https://doi.org/10.1016/j.mssp.2017.10.001.

[43] Z. Kása, E.E. Almási, K. Hernádi, T. Gyulavári, L. Baia, G. Veréb, Z. László, Z. Pap, New insights into the photoactivity of shape-tailored BiVO4 semiconductors via photocatalytic degradation reactions and classical reduction processes, Molecules 25 (2020) 4842, https://doi.org/:10.3390/molecules25204842.

[44] E. Bárdos, A.K. Király, Z. Pap, L. Baia, S. Garg, K. Hernádi, The effect of the synthesis temperature and duration on the morphology and photocatalytic activity of BiOX (X = Cl, Br, I) materials, Appl. Surf. Sci. 479 (2019) 745–756, https://doi.org/10.1016/j.apsusc.2019.02.136.

[45] E.V. Timakova, L.I. Afonina, N.V. Bulina, S.S. Shatskaya, Y.M. Yukhin, V. A. Volodin, Synthesis of basic bismuth(III) oxalate by precipitation from nitrate solutions, Russ. J. Appl. Chem. 90 (2017) 1040–1046, https://doi.org/:10.1134/S1070427217070035.

[46] K. Xiao, N. Tian, Y. Guo, H. Huang, X. Li, Y. Zhang, Facile synthesis, electronic structure and photocatalytic activity of a novel Bi-based hydroxyl oxalate Bi(C₂O₄)OH, Inorg. Chem. Commun. 52 (2015) 5–8, https://doi.org/10.1016/j.inoche.2014.12.005.

[47] S. Abraham, S.T. David, R. Bennie, J. Chellappa, S.K.Devendhar Singh, Eco-friendly and green synthesis of BiVO4 nanoparticle using microwave irradiation as photocatalyst for the degradation of Alizarin Red S, J. Mol. Struct. 1113 (2016) https://doi.org/:10.1016/j.molstruc.2016.01.053.

[48] Z. Liu, X. Xu, J. Fang, X. Zhu, J. Chu, B. Li, Microemulsion synthesis, characterization of bismuth oxyiodine/titanium dioxide hybrid nanoparticles with outstanding photocatalytic performance under visible light irradiation, Appl. Surf. Sci. 258 (2012) 3771–3778, https://doi.org/10.1016/j.apsusc.2011.12.025.

[49] X. Xue, W. Wang, H. Fan, Z. Xu, I. Pedruzzi, P. Li, J. Yu, Adsorption behavior of oxalic acid at water–feldspar interface: experiments and molecular simulation, Adsorption 25 (2019) 1191–1204, https://doi.org/10.1007/s10450-019-00111-8.

[50] S.K. Poznyak, A.I. Kulak, Photoelectrochemical properties of bismuth oxyhalide films, Electrochim. Acta 35 (1990) 1941–1947, https://doi.org/10.1016/0013-4686(90)87103-9.

[51] T. Jedsukontorn, V. Meeyoo, N. Saito, M. Hunsom, Effect of electron acceptors H₂O₂ and O₂ on the generated reactive oxygen species 1O₂ and OH in TiO₂-catalyzed photocatalytic oxidation of glycerol, Chin. J. Catal. 37 (2016) 1975–1981, https://doi.org/10.1016/S1872-2067(16)62519-6.

[52] P. Nekovář, D. Schrötterová, Extraction of V(V), Mo(VI) and W(VI) polynuclear species by primene JMT, Chem. Eng. J. 79 (2000) 229–233, https://doi.org/10.1016/S1385-8947(00)00207-2.

[53] J. Coca, F.V. Díez, M.A. Morís, Solvent extraction of molybdenum and tungsten by Alamine 336 and DEHPA, Hydrometallurgy 25 (1990) 125–135, https://doi.org/10.1016/0304-386X(90)90034-Y.